Cement and Concrete Research 40 (2010) 1265–1270

Contents lists available at ScienceDirect

Cement and Concrete Research

journal homepage: http://ees.elsevier.com/CEMCON/default.asp

Application of synchrotron microtomography for pore structure characterization of deteriorated cementitious materials due to leaching

T. Sugiyama [a,*], M.A.B. Promentilla [a], T. Hitomi [b], N. Takeda [b]

[a] Environmental Material Engineering Laboratory, Graduate School of Engineering, Hokkaido University, Kita 13 Nishi 8 Kita-ku, Sapporo 060-8628, Japan
[b] Technical Research Institute, Obayashi Corp., Japan

ARTICLE INFO

Article history:
Received 19 May 2009
Accepted 6 October 2009

Keywords:
Pore structure
Synchrotron-based X-ray computed microtomography
Random walk simulation
Calcium leaching
Cement paste

ABSTRACT

Deteriorated mortars and cement pastes ($w/c = 0.50$) were prepared by an accelerated leaching test using electrochemical migration technique. This technique enabled the reduction of the CaO/SiO_2 molar ratio to less than 2.0. Non-destructive three-dimensional imaging of the internal microstructure of the deteriorated cement matrix in hardened cement paste and mortar was performed using synchrotron X-ray computed microtomography at SPring-8, Japan. After image analysis at a spatial resolution of 0.5 μm/voxel the microtomographic images successfully visualized increased pore spaces in the deteriorated cement matrix with the effective porosity ranging from 0.31 to 0.38. In addition the diffusion tortuosity in the pore space derived from random walk simulation was also evaluated as a pore structure-transport parameter. Indications suggest that the deterioration of the cement matrix due primarily to the dissolution of portlandite decreases the diffusion tortuosity to a single digit as the degree of pore connectivity becomes larger at the submicron scale.

1. Introduction

Extremely long-term performance of concrete structures to be constructed deep underground for radioactive waste repository will be in danger by groundwater attack. It has been reported that the pore structure in cement paste was changed by contact with ion-exchange water due to dissolution [1]. In this way leaching of cement hydrates could degrade mechanical characteristics and transport properties in the cementitious materials [2,3]. Pore structure characteristics of cementitious materials are often evaluated by mercury intrusion porosimetry and scanning electron microscopy. However, most of these techniques assume the pore geometry in the interpretation of results, and are either invasive or limited to two-dimensional (2D) information.

Recently microtomography with synchrotron radiation as the X-ray source has been applied by various researchers [4–9]. Resolution for the image analysis of microstructure in cementitious materials may not be sufficient even in the use of the synchrotron microtomography. However, considering recent development of the synchrotron microtomography that enables increasing the resolution up to 0.5 μm/voxel at the SPring-8 facility in Japan it is expected that pore structure analysis for deteriorated cement matrix in hardened cement paste will provide new evidence on the microstructure change. In addition quantitative evaluation on the pore structure of deteriorated cementitious materials is necessary to implement so as to predict the extremely long-term safety performance using a simulation model [11,12].

In this study, a mortar and cement paste ($w/c = 0.50$) was subjected to an accelerated leaching test using electrochemical migration technique. This is because of the fact that the leaching of cement hydrates progresses extremely slowly until a given deterioration is manifested. Then this technique simulates the long-term deterioration behavior of the cement matrix due to calcium leaching when in contact with water (13). Non-destructive three-dimensional imaging of the internal microstructure of the deteriorated cement matrix in hardened cement paste and mortar was performed using synchrotron X-ray computed microtomography at SPring-8, Japan (9,10). The CaO/SiO_2 molar ratio of the specimens was also measured from EPMA (electron probe microanalysis) studies. In this paper, the diffusion tortuosity in the pore space derived from random walk simulation was also evaluated as a pore structure-transport parameter associated with the 3D-microgeometry of the pore space in deteriorated samples.

2. Materials and methods

2.1. Specimen preparation and experimental procedure

A mortar and cement paste with a water to cement ratio of 0.5 was prepared. The cement used was an ordinary Portland cement (OPC) designated as JIS R5210 that is commercially available in Japan. By mass, this type of cement contains 67.8% of CaO, 21.3% of SiO_2, 3.80% of

* Corresponding author. Tel./fax: +81 11 706 6178.
E-mail address: takaf@eng.hokudai.ac.jp (T. Sugiyama).

0008-8846/$ – see front matter © 2009 Elsevier Ltd. All rights reserved.
doi:10.1016/j.cemconres.2009.10.009

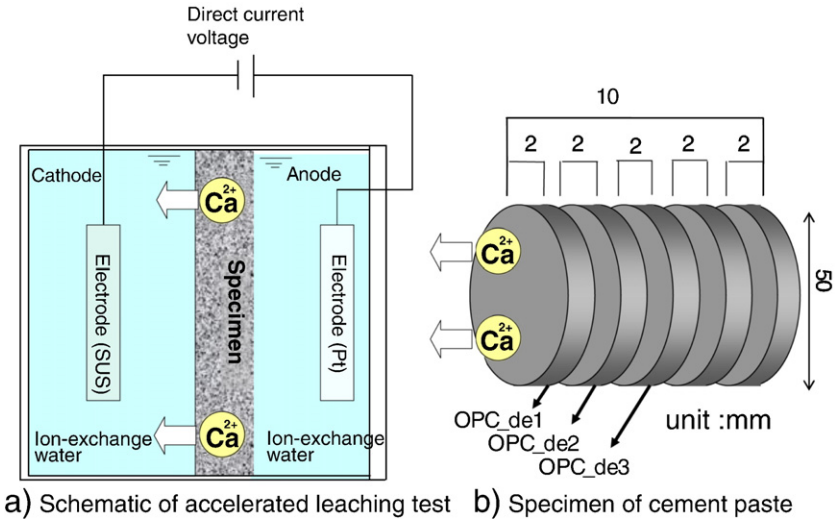

Fig. 1. Electrochemical acceleration test.

Al_2O_3, 2.41% of Fe_2O_3, and 2.20% of SO_3. The fineness of the OPC in terms of Blaine specific surface area is 3200 cm^2/g. As for the mortar specimen, a sand (maximum particle size of 210 μm) to cement ratio of 2.0 was used in preparing the mix. To prevent segregation, chemical admixtures were also added to the mixes of cement paste and mortar. The size of specimen prepared was 50 mm in diameter and 100 mm in length, and was cured for 20 weeks prior to the accelerated leaching tests. After curing, a 10-mm thick specimen was cut from the specimen for accelerated leaching tests.

The experimental set-up described in Ref. [13] and [14] was used for the accelerated leaching test as shown in Fig. 1. The 10-mm thick specimen was placed between two acryl-made compartments, each containing 1 l of ion-exchanged water. One compartment has an anode made of platinum (Pt) and the other has a stainless steel (SUS) cathode. These two electrodes are connected via an electrical DC power source to provide a potential gradient across the specimen. The application of electrical field accelerates the dissolution of hydrated cement products such as portlandite and the cations such as the Ca^{2+} move rapidly to the cathode side [13,14]. In this study, mortar and cement paste specimens were subjected to accelerated leaching test for 13 weeks prior to microtomographic examination.

After the leaching test, a 10×15 mm plate was prepared from the deteriorated cement paste. The surface of the plate was embedded with resin and polished for electron probe microanalysis (EPMA). The pixel size was 20 μm and the acceleration voltage was 15 kV with a counting interval of 50 ms. In this way C/S ratios in the target surface of the cement paste under the observation were determined. For microtomographic studies, OPC_de1, OPC_de2, and OPC_de3 refer to the portions that were cut 2 mm, 4 mm, and 6 mm from the surface layer of cement paste that was exposed in the cathode side. As for the deteriorated mortar (DM), a portion that corresponds to the cathode side was also prepared. From each cut portion, a shard of about 1 mm at its greatest width and 1 mm in length was obtained to examine the internal pore structure with synchrotron-based microtomography. In addition, a specimen from cement paste (OPC_nde) and mortar (Non-DM) not subjected to the accelerated leaching test was also prepared for microtomographic examination.

2.2. Image acquisition, processing and analysis

Microtomographic images were acquired at high spatial resolution using the X-ray CT system (BL20XU/BL47XU) at SPring-8 (Super Photon ring-8 GeV), Hyogo, Japan, which is one of the world's largest third generation synchrotron radiation facilities. A schematic illustration of synchrotron microtomography is shown in Fig. 2. Details of this experimental set-up are described elsewhere [15].

In this study, the X-ray energy was set to a value of 15 keV. Using a high precision rotation stage, 1500 projection images were taken at different views with an exposure time of 0.30 s per projection and angle step of 0.12° through the 180° rotation. The transmitted images are then detected by an X-ray image detector which consists of a thin scintillator, optic system and CCD camera. Tomographic reconstruction is performed using a public domain computer program in use at SPring-8, which employs the convolution back projection algorithm to generate the slice or cross-sectional images.

The stack of these slices provides the reconstructed volumetric data of the scanned object. In this study, the reconstructed 3D-image data set was composed of 1300 contiguous grayscale images where each slice image contained 2000×2000 voxels (volume element or 3D pixel). The effective size of a cubic voxel in the CT image is 0.5 μm.

Normalization or contrast stretching was applied to the whole stack of the reconstructed slices to even out the brightness and contrast variation between the slices, as well as, to enhance the contrast in the said images. In the normalization process, the set of images was also

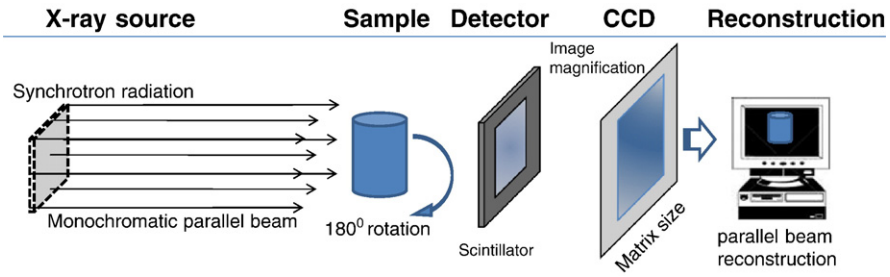

Fig. 2. X-ray CT system at SPring-8, Japan.

down-sampled from 16-bit to 8-bit grayscale images resulting in a smaller image file size. To reduce the computational time, a cubic volume of interest (VOI) of 300^3 voxels was then extracted from the original data set for further image analysis.

SLICE, a basic 3D-image analysis program developed in SPring-8, was used for pore segmentation and cluster labeling of the images in the VOI. For pore segmentation, global thresholding was used to separate the pore from the "solid" matrix by defining the range of grayscale value (GSV) associated with pore voxels. The lower bound of GSV associated with pore voxels was set to 0 while the upper bound is set to the pore threshold value on the basis of transition point in segmented porosity-threshold dependency curve [9]. At this threshold value, the segmented porosity started to increase rapidly wherein the boundary between pore and the solid matrix is most likely to be segmented as pore space.

After pore segmentation, pore connectivity analysis was then performed on the basis of cluster labeling that is commonly described in percolation theory [16]. In this analysis, pore voxels are considered connected to form the "pore cluster" when these voxels are in face-to-face contact with each other. In other words, two voxels are considered to be connected when the said pore voxel shares a common face with the other whereas if the pore voxels are in contact only at the vertex or edge, then the voxels are considered to be disconnected. This cluster multiple labeling procedure allowed us then to identify the largest percolating pore cluster if any from the other smaller isolated or dead-end pore clusters. The criterion we used to define percolation here is when this pore cluster contains voxels that are connected to the six faces of the cubic VOI. Thus, the largest percolating pore cluster is assumed to be the connected pores that most likely contribute to the macroscopic transport in the cement matrix.

After extracting the largest percolating pore space, random walk simulation was performed in the digitized pore space to probe the pore geometry and quantify the diffusion tortuosity. Diffusion tortuosity is defined as the ratio of the self-diffusion coefficient (D_o) of non-sorbing walkers in free space to the long-time self-diffusion coefficient (D_∞) of these walkers in pore space. This technique has been applied to microtomographic images of geologic materials [17,18] and more recently, to that of hardened cement pastes of different ages of curing [9,10]. In this study, a 3D random walk algorithm implemented in Mathematica was employed to compute the mean square displacement of random walkers in a simple cubic lattice with mirror boundaries. The details of this algorithm are described elsewhere [17,18].

3. Results and discussion

3.1. Image analysis for quantification of pore structure

Fig. 3 describes the representative slices obtain from each specimen after the normalization process. As shown in this figure, the background or surrounding air is imaged as very dark voxels in contrast to the foreground or the scanned object. It should be noted that the brightness intensity of each voxel in the microtomographic images is proportional to the measured X-ray attenuation coefficient that is strongly correlated with density. Accordingly, the darker voxels in the reconstructed grayscale image correspond to low density phases (e.g., air voids or pores), whereas the brighter voxels denote the high density phases (e.g., anhydrous cement). In the microtomographic images of the cement paste (Fig. 3c–f), the light to medium gray voxels that are distributed all over the cross-section are most likely associated with the hydrated cement products. On the other hand, the light to dark gray patch shown in the microtomographic image of mortar specimens (see Fig. 3a and b) is most likely associated with the sand particles.

Fig. 4 describes an example of the VOI and the corresponding 3D images after pore segmentation and cluster labeling. The binary images after pore segmentation (see Fig. 4b) were used to quantify the segmented porosity in the VOI by dividing the number of pore voxels (black) by the total number of voxels (300^3) in the VOI. Results from the cluster multiple labeling showed 35,176 individual pore clusters in the said VOI. In Fig. 4c, the largest pore cluster that is percolating in three orthogonal directions is imaged as blue voxels whereas the other 35,175 smaller pore clusters that are either isolated

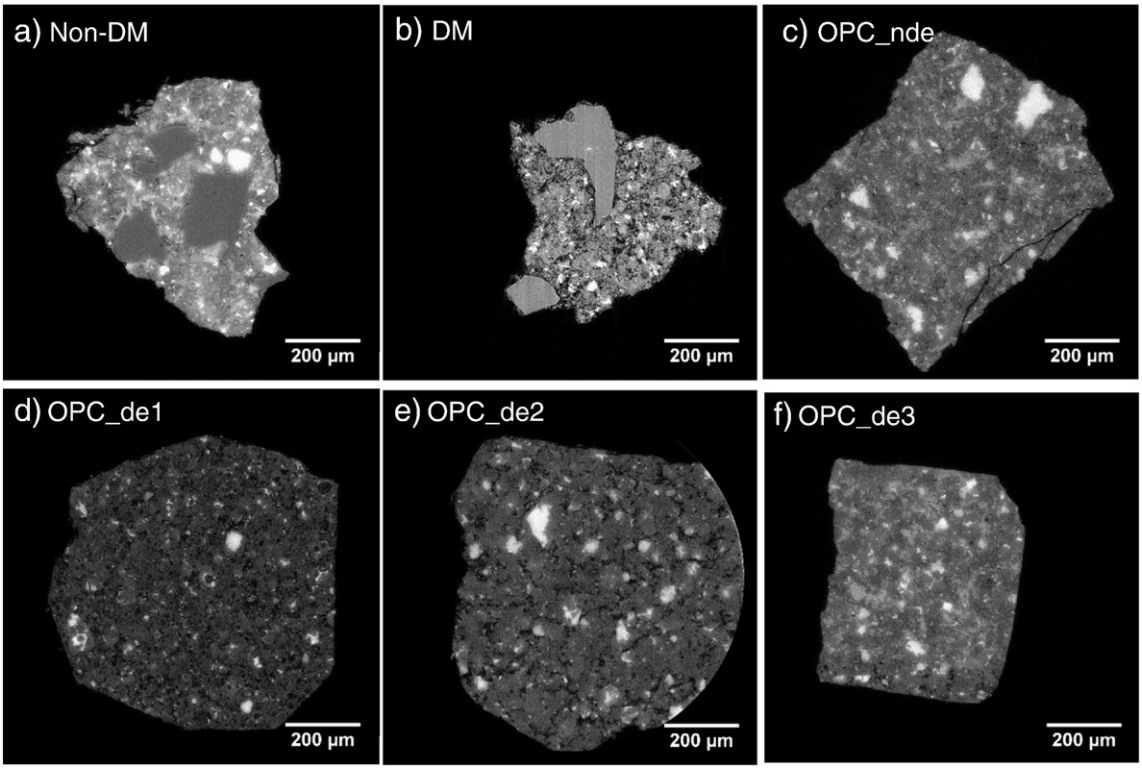

Fig. 3. Cross-sectional slices with the normalized reconstructed 8-bit grayscale image (2000 × 2000 voxels of 0.5 μm size).

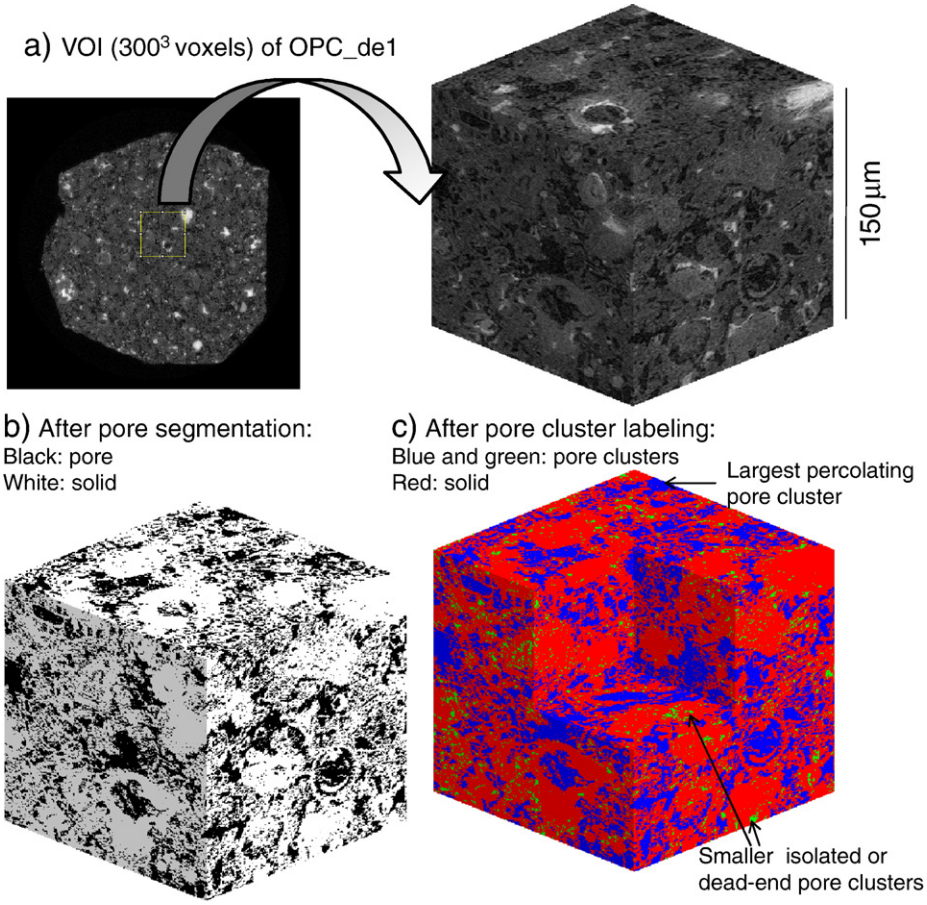

Fig. 4. Volume of Interest (VOI) extracted from original data set and visualization of output from pore segmentation and cluster labeling.

or dead-end pores are imaged as green voxels. Then, the degree of pore connectivity was quantified by dividing the number of pore voxels in the largest percolating pore cluster by the total number of pore voxels in the VOI. Thus, a pore connectivity of 1.0 indicates that all pore voxels in the segmented porosity are connected to each other. Furthermore, we defined the effective porosity that is open and percolating in three orthogonal directions by multiplying the degree of pore connectivity to the segmented porosity. Table 1 summarizes the results from pore segmentation and connectivity analysis of the VOI of each specimen. Region of the cement paste was chosen for the VOI analysis for mortar specimens. It appeared that the porosity and connectivity of Non-DM and DM showed similar results to those for OPC_nde and OPC_de1, respectively.

It should be noted that these results are dependent on the digital resolution of the microtomographic images. A greater number of pores may not be detected as pores become finer (and becomes much less than 0.5 µm) in specimens that age considerably. Thus, this obviously affected the pore connectivity analysis of non-deteriorated specimens (Non-DM and OPC_nde) such that no percolation of pores was observed. On the other hand, a remarkable increase of porosity and degree of pore connectivity in cement matrix were observed for both mortar (DM) and cement paste (e.g., OPC_de1) in contact with water at the cathode side. This could be explained by the increased volume of larger pores of about 0.5 µm or more. Having considered that the size of portlandite in the form of crystal is around a few micrometers [1] we could say that the pores resolved from the microtomographic images of deteriorated cement matrix are caused by the dissolution of portlandite. Thus, synchrotron microtomography is a powerful tool to characterize the 3D pore structure associated with the dissolution of portlandite as calcium ions leached out from the cement matrix.

As shown in Fig. 5, the changes in CaO/SiO_2 molar ratio (referred to hereafter as the C/S ratio) through the cross-section indicated that deterioration due to calcium leaching becomes less and less at regions farther from the surface layer (cathode side) in contact with water. It should be noted that this profile of C/S ratio is not for the C–S–H but for the cement paste matrix under its line profile observation by the EPMA

Table 1
Results from pore segmentation and connectivity analysis.

Specimen	Segmented porosity	Degree of pore connectivity	Effective porosity
Non-DM	0.04	No percolation	No percolation
DM	0.39	0.98	0.38
OPC_nde	0.09	No percolation	No percolation
OPC_de1	0.33	0.93	0.31
OPC_de2	0.21	0.83	0.17
OPC_de3	0.14	0.67	0.09

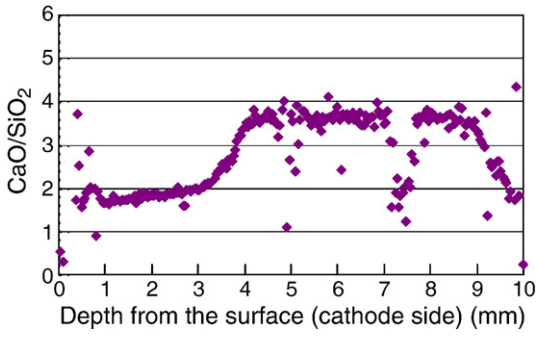

Fig. 5. Profile of C/S molar ratio by EPMA.

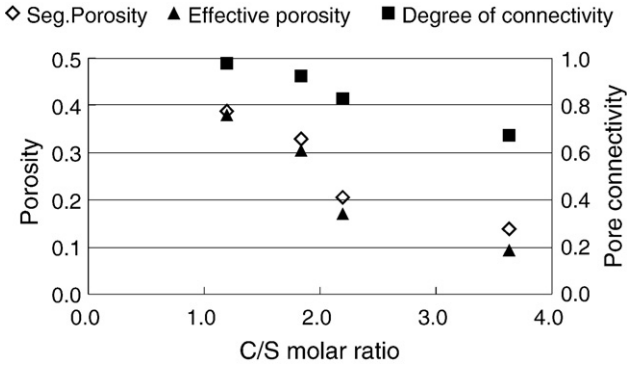

Fig. 6. Relationship between porosity and C/S molar ratio.

within about 3 mm from the cathode the C/S ratios are reduced to less than 2.0. This deterioration pattern seems to agree with the changes in computed porosity and pore connectivity through the surface layer to the inner portion of the deteriorated cement pastes (OPC_de1, OPC_de2, and OPC_de3). The results (see Table 1) indicated that a decreasing volume of connected larger pores associated with portlandite dissolution is detected as the region becomes farther from the cathode side. Fig. 6 illustrates the relationship of porosity and pore connectivity to the C/S ratio in deteriorated cementitious material.

3.2. Diffusion tortuosity by random walk simulation

Output from the random walk simulation in the largest percolating pore cluster is shown in Fig. 7. A random walk simulation was also performed in free space (i.e., porosity = 100%) of the same VOI size to serve as a reference. Fig. 7a shows the sample trajectory of a walker in the 3D pore space (OPC_de1). In this figure, the black lines represent the

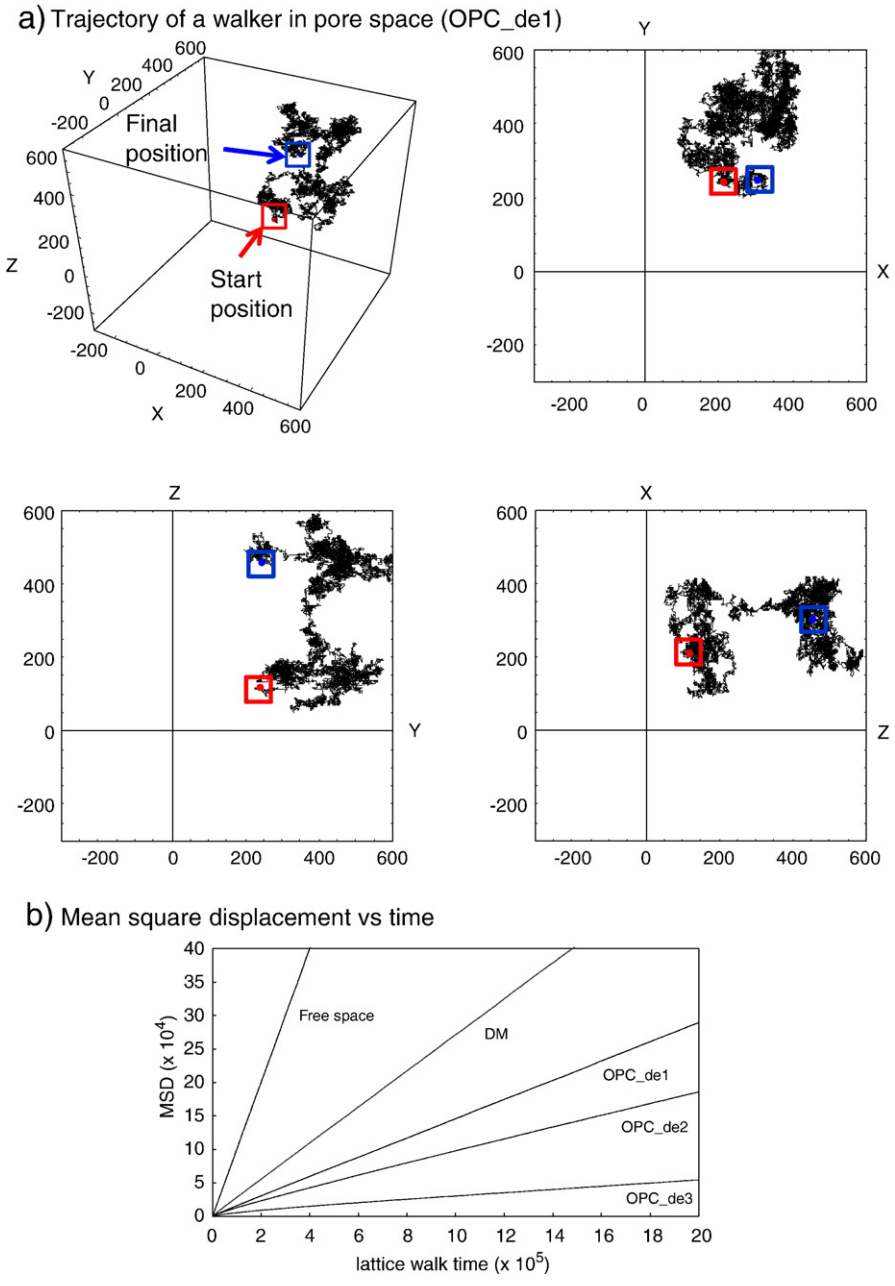

Fig. 7. Results from random walk simulation.

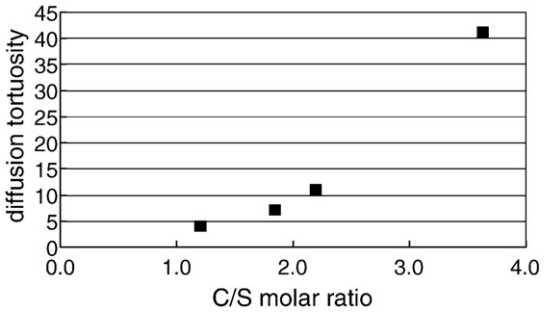

Fig. 8. Relationship between diffusion tortuosity and C/S molar ratio.

path of the walker in the 3D view of the lattice, as well as, the projected trajectory in three orthogonal planes. The red dot is the starting position chosen randomly for this specific walker whereas the blue dot is its final position after the final step (2 million steps) of lattice walk. In Fig. 7b, the dimensionless mean square displacement (MSD) averaged over 50,000 walkers is plotted against the time (t) of lattice walk (maximum of 2 million steps). At 100% porosity, the mean square displacement of walkers was observed to be directly proportional to the time of the lattice walk as this indicates unconstrained diffusion in free space. On the other hand, results from random walk simulation in pore space show a curve of MSD against time as this indicates restricted diffusion resulting in a reduced self-diffusion coefficient of the walkers as they probe the tortuosity of the pore space. At long-time diffusion, the slope of MSD against time would correspond to the inverse (diffusion) tortuosity of the pore space.

As expected, the diffusion tortuosity in free space was computed to be equal to 1.0 whereas the tortuosity values in the pore space of the DM, OPC_de1, OPC_de2, and OPC_de3 were computed to be equal to 4, 7, 11 and 41, respectively. Note that the diffusion tortuosity was not evaluated for non-deteriorated mortar and cement paste because no percolation of the pores was observed. Fig. 8 illustrates the relationship of tortuosity to the C/S ratio in deteriorated cementitious material. Indication suggests that complete dissolution of portlandite at the surface in contact with water would have reduced dramatically the diffusion tortuosity as more pores of larger size become connected in contrast to that of the inner layer farther from the cathode side.

4. Conclusions

Based on this research the following conclusions are drawn.

(1) Synchrotron microtomography investigation reveals a significant increase in the pore volume resulting in the increased degree of pore connectivity in the cement matrix in the deteriorated cement paste and mortar.
(2) Effective porosity accounted for by percolating pores increases up to 0.31–0.38 by leaching of cement hydrates.
(3) Diffusion tortuosity obtained from random walk simulation is reduced largely to a single digit as CaO/SiO_2 molar ratio decreases to less than 2.0.

Acknowledgments

Part of this present research work was funded by the Japan Society for the Promotion of Science, Grant-in-Aid for Scientific Research (B) (Research No.: 19360193). The synchrotron radiation experiments were performed at the BL20XU in SPring-8 with the approval of the Japan Synchrotron Radiation Research Institute (JASRI) (Proposal No. 2007A1951-NL-np).

References

[1] K. Haga, M. Shibata, M. Hironaga, S. Tanaka, S. Nagasaki, Change in pore structure and composition of hardened cement paste during the process of dissolution, Cem. Con. Res. 35 (5) (2005) 943–950.
[2] C. Carde, R. Francois, Effect of the leaching of calcium hydroxide from cement paste on mechanical and physical properties, Cem. Concr. Res. 274 (1997) 539–550.
[3] H. Saito, A. Deguchi, Leaching tests on different mortars using accelerated electrochemical method, Cem. Concr. Res. 30 (11) (2000) 1815–1825.
[4] D.P. Bentz, D.A. Quenard, H.M. Kunzel, J. Baruchel, F. Peyrin, N.S. Martys, E.J. Garboczi, Microstructure and transport properties of porous building materials. II: Three-dimensional X-ray tomographic studies, Mat. Struct. 33 (2000) 147–153.
[5] Hitomi, T., Mita, Y., Saito H., Takeda, N., Observation of Fine Structure of Mortar Using X-ray CT Images at SPring-8, Proceedings of Annual Conference of Japan Concrete Institute, 26(1)(2004), pp. 645–650 (in Japanese).
[6] L. Helfen, F. Dehn, P. Mikulik, T. Baumbach, Three-dimensional imaging of cement microstructure evolution during hydration, Adv. Cem. Res. 17 (3) (2005) 103–111.
[7] N. Burlion, D. Bernard, Da Chen, X-ray microtomography: application to microstructure analysis of a cementitious material during leaching process, Cem. Con. Res. 36 (2006) 346–357.
[8] E. Gallucci, K. Scrivener, A. Groso, M. Stampanoni, G. Margaritondo, 3D experimental investigation of the microstructure of cement pastes using synchrotron X-ray microtomography, Cem. Con. Res. 37 (2007) 360–368.
[9] A.B.M. Promentilla, T. Sugiyama, T. Hitomi, N. Takeda, Characterizing the 3D pore structure of hardened cement paste with synchrotron microtomography, J. Adv. Concr. Tech. 6 (2) (2008) 273–286.
[10] A.B.M. Promentilla, T. Sugiyama, T. Hitomi, N. Takeda, Quantification of tortuosity in hardened cement pastes using synchrotron-based X-ray computed microtomography, Cem. Con. Res. 39 (2009) 548–557.
[11] T. Sugiyama, W. Ritthichauy, Y. Tsuji, Simultaneous transport of chloride and calcium ions in hydrate cement systems, J. Adv. Concr. Tech. 1 (2) (2003) 127–138.
[12] T. Sugiyama, W. Ritthichauy, Y. Tsuji, Experimental investigation and numerical modeling of chloride penetration and calcium dissolution in saturated concrete, Cem. Con. Res. 38 (2008) 49–67.
[13] H. Saito, S. Nakane, S. Ikari, A. Fujiwara, Preliminary experimental study on the deterioration of cementations materials by an acceleration method, Nucl. Eng. Des. 138 (1992) 151–155.
[14] H. Saito, S. Nakane, Comparison between diffusion test and electrochemical acceleration test for leaching degradation of cement hydration products, ACI Mater. J. 96 (2) (1999) 208–212.
[15] K. Uesugi, Y. Suzuki, N. Yagi, A. Tsuchiyama, T. Nakano, Development of high spatial resolution X-ray CT system at BL47XU in SPring-8, Nuclear Instruments and Methods I Physics Research A 467–468 (2001) 853–856.
[16] S. Ikeda, N. Nakano, Y. Nakashima, Three-dimensional study on the interconnection and shape of crystals in a graphic granite by X-ray CT and image analysis, Mineral. Mag. 64 (5) (2000) 945–959.
[17] Y. Nakashima, T. Nakano, K. Nakamura, K. Uesugi, A. Tsuchiyama, S. Ikeda, Three-dimensional diffusion of non-sorbing species in porous sandstone: computer simulation based on X-ray microtomography using synchrotron radiation, J. Contam. Hydrol. 74 (2004) 253–264.
[18] Y. Nakashima, S. Kamiya, Mathematica programs for the analysis of three-dimensional pore connectivity and anisotropic tortuosity of porous rocks using X-ray microtomography, J. Nucl. Sci. Technol. 44 (9) (2007) 1233–1247.